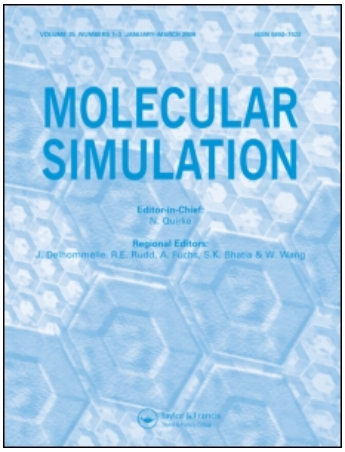

Molecular Simulation

Publication details, including instructions for authors and subscription information:
http://www.informaworld.com/smpp/title~content=t713644482

Structural properties of amorphous $Al_2O_3 \cdot 2SiO_2$ nanoparticles

N. N. Linh[a]; V. V. Hoang[a]
[a] Department of Physics, Institute of Technology, National University of HochiMinh City, HochiMinh City, Vietnam

To cite this Article Linh, N. N. and Hoang, V. V.(2008) 'Structural properties of amorphous $Al_2O_3 \cdot 2SiO_2$ nanoparticles', Molecular Simulation, 34: 1, 29 — 34
To link to this Article: DOI: 10.1080/08927020801930521
URL: http://dx.doi.org/10.1080/08927020801930521

Molecular Simulation
Vol. 34, No. 1, January 2008, 29–34

Taylor & Francis
Taylor & Francis Group

Structural properties of amorphous $Al_2O_3{\cdot}2SiO_2$ nanoparticles

N.N. Linh* and V.V. Hoang

Department of Physics, Institute of Technology, National University of HochiMinh City, 268 Ly Thuong Kiet Street, District 10, HochiMinh City, Vietnam

(Received 14 July 2007; final version received 14 January 2008)

Structural properties of amorphous $Al_2O_3{\cdot}2SiO_2$ (denoted as AS_2) spherical nanoparticles have been studied in a model with different sizes of 2, 3 and 4 nm under non-periodic boundary conditions with the Born–Mayer type pair potentials via molecular dynamics (MD) simulation. We studied structural properties via the partial radial distribution functions (PRDFs), coordination number distributions, bond-angle distributions and interatomic distances. Moreover, the radial density profile in nanoparticles was found. Calculations show that size effects on structure of a model are significant and calculated data differ from those obtained previously in the bulk counterpart. We found that if the size is larger than 3 nm, amorphous AS_2 nanoparticle has a distorted tetrahedral network structure with the mean coordination number $Z_{Al-O} \approx 4$ and $Z_{Si-O} \approx 4$. The existence of triclusters in nanoparticles and size dependence of tricluster composition have been found and discussed. Furthermore, we also showed surface structure and surface energy of nanoparticles.

Keywords: amorphous aluminosilicate; nanoparticles; nanoscale materials

PACS numbers: 61.46-w; 78.55.Qr; 61.43.Bn

1. Introduction

Aluminosilicate nanoparticles attracted great interest for the years because of their important applications in technology, i.e. they were used in drug storage and release, biomedicine, optics and electronics or in the adsorption of arsenic in order to remove them from aqueous environments [1–3]. In particular, aluminosilicate nanoparticles containing 9.0–20 nm mesopores were prepared for cracking of very large hydrocarbons in oil industry [4–5]. Therefore, the microstructure of liquid and amorphous aluminosilicate nanoparticles have aroused a great interest from both experiments and computer simulations. On the other hand, the amorphous nanoparticulate aluminosilicate 3/2-mullite precursor has been synthesized, and the sols contained 2-nm particles of Q^3(3Al) silica species together with six-coordinated alumina were found, which were suggested as an allophane-like structure nanoparticles. These sols were characterized by small-angle X-ray scattering, dynamic light scattering, X-ray diffraction, ^{27}Al and ^{29}Si MAS nuclear magnetic resonance spectroscopy, and differential thermal analysis [6]. In addition, aluminosilicate nanoparticles have been also produced in the forms of powder, sol–gel and composite coating particles [7,8]. However, detailed information on an atomistic level can be provided just via using computer simulations. Indeed, the local description about zeolites versus aluminosilicate clusters was shown by the force field calculations on extended systems and by *ab initio* quantum chemical calculations on ring structures. It reveals that the relation and energy content of neutral-framework silicates were determined by that of the smallest substructures [9]. In contrast, it is worth noting that there are several works related to other oxide nanoparticles such as SiO_2, Al_2O_3, TiO_2 and Fe_2O_3 (see for example in [10–13]). Detailed information about local structure of amorphous AS_2 nanoparticles has not been obtained yet although such properties of aluminosilicate bulk counterpart have been under intensive investigations by both experimental and numerical methods [14–26]. The fact, liquid and amorphous AS_2 models under periodic boundary conditions, i.e. the bulk counterpart, have been accurately described with the Born–Mayer potential via MD simulations and their structural properties agreed well with the experiments [27–29]. In particular, the liquid and amorphous AS_2 have relatively large amount of five- and six-fold coordinated Al atoms to oxygen in addition to AlO_4 and SiO_4 units [18,19,25,27–29]. Therefore, it motivates us to carry out the systematic analysis of structure of amorphous AS_2 nanoparticles compared with those observed in the bulk counterpart. In addition, surface effects on structure and properties of amorphous nanoparticles with different sizes have been analyzed in details.

*Corresponding author. Email: ngoclinh84phys@yahoo.com

ISSN 0892-7022 print/ISSN 1029-0435 online

DOI: 10.1080/08927020801930521
http://www.informaworld.com

2. Calculation

The simulations were done in a spherical model under non-periodic boundary conditions with the sizes of 2, 3 and 4 nm, which contains the number of atoms corresponding to the real density of $2.6\,\mathrm{g\,cm^{-3}}$ for amorphous AS_2 [30]. The interatomic potentials of the Born-Mayer type, which were successfully used in our previous works for liquid and amorphous $Al_2O_3{\cdot}2SiO_2$ [27–29], have been used in this work and their form is given below:

$$U_{ij} = Z_i Z_j \frac{e^2}{r} + B_{ij} \exp\left(-\frac{r}{R}\right) \qquad (1)$$

Where the terms present Coulomb and repulsive energies, respectively. Here r denotes the distance between the centers of ith and jth ions, and Z_i, Z_j are the charges of ions: $Z_{Al} = +3$, $Z_{Si} = +4$, $Z_O = -2$. B_{ij} and R_{ij} are the parameters accounting for the repulsion of the ionic shells. The values $B_{AlAl} = 0$, $B_{AlSi} = 0$, $B_{SiSi} = 0$, $B_{AlO} = 1779.89\,\mathrm{eV}$, $B_{SiO} = 1729.50\,\mathrm{eV}$, $B_{OO} = 1500\,\mathrm{eV}$, and $R_{ij} = 29\,\mathrm{pm}$. More details about these potentials can be found in [27–29,31,32]. Coulomb interactions were taken into account by mean of Ewald–Hansen method. We use the Verlet algorithm with the MD time step 1.6 fs. We first placed randomly N atoms in a sphere of fixed radius and the configuration has been relaxed for 50,000 MD steps at 7000 K, after that temperature of the system was decreased linearly in the time from 7000 K to 350 K by the cooling rate $\gamma = 4.375 \times 10^{13}\,\mathrm{K\,s^{-1}}$. All calculations were done at constant volume. Structural quantities were calculated after relaxation for 80 ps at this temperature [27].

3. Results and discussions

In order to obtain the size dependence of structure of amorphous AS_2 nanoparticles, in this work we show the structural characteristics of well-relaxed models at 350 K. The first quantity we would like to discuss here is the PRDF for different atomic pairs. As shown in Figure 1 and Table 1, we can see that the position of the first peaks in PRDFs changes slightly with particles size. It has the value smaller than that for the bulk with an exception for Al—Al pair. In contrast, the peaks in PRDF of nanoparticles are boarder and higher than those for the bulk indicating that the structure of amorphous nanoparticles is more heterogeneous than that of the bulk and probably due to the contribution of surface structure [11]. In addition, it also pointed out that the method of linkage of structural units-polyhedra such as AlO_n and SiO_n in amorphous AS_2 nanoparticles differs from that of the bulk because it essentially defines intermediate range order at scales from roughly 4 to 10 Å in network of aluminosilicates [33]. Therefore, one can infer that size effects on intermediate range order are more pronounced than those on the local range one and possibly, it can cause differences in method of linkage of SiO_n and AlO_n in nanoparticles (Figure 1). Analogously, it is essential to notice that PRDF for the Al—Al pair of nanoparticles is also splitting into two peaks like those

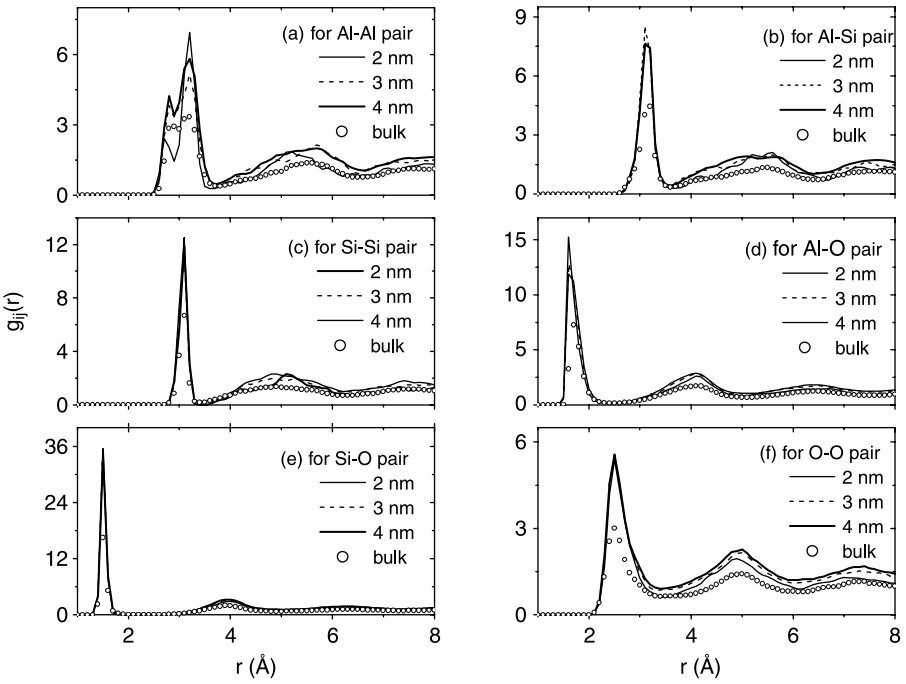

Figure 1. Radial distribution functions of amorphous AS_2 nanoparticles and bulk [27] at 350 K.

Table 1. Structural characteristics of amorphous AS_2 at 350 K; R_{ij} – position of the first peaks in PDRFs; Z_{ij} – the average coordination number.

	R_{ij} (Å)						Z_{ij}			
Materials	Al—Al	Al—Si	Si—Si—	Al—O	Si—O	O—O	Al—O	O—Al	Si—O	O—Si
2 nm	3.19	3.14	3.09	1.62	1.50	2.50	3.77	1.51	4.05	1.36
3 nm	3.20	3.12	3.08	1.64	1.50	2.50	4.01	1.61	4.03	1.35
4 nm	3.19	3.14	3.08	1.64	1.50	2.50	4.10	1.67	4.08	1.39
Amorphous bulk models [27]	3.17	3.16	3.09	1.72	1.51	2.50	4.57	1.30	4.18	1.19
Exp. for the amorphous bulk [20,26]				1.71 1.77			4.54		~4	

observed in the bulk. This means that in network structure of amorphous AS_2 nanoparticles, there are two different characteristic length scales r_1 and r_2 for the distance between nearest Al neighbors. These two scales should be also reflected in the geometry of the AlO_4 tetrahedra and two connected tetrahedra for which the Al atoms are located at a distance r_1 from each other may have a different geometry from two connected tetrahedra where the two Al atoms in the centre are at distance of around r_2. It may be related to the existence of small-membered rings like those discussed in [30].

We found that Al—O bond length in nanoparticles is smaller than that in the bulk counterpart (see Table 1). As discussed in previous simulations and experiments [22,29], the lager value obtained for Al—O bond length in AS_2 bulk is related to the larger number of over-coordinated structural units such as AlO_5 and AlO_6 in the bulk compared with that in nanoparticles (i.e. $Al^{V} - O = 1.83$ Å, $Al^{VI} - O = 1.88$ Å) [22,34]. The mean coordination number for Al—O and Si—O pairs in amorphous nanoparticles, however, is smaller than that for the bulk and it is closer to those for the ideal tetrahedral coordinated Al—O and Si—O networks [31,32]. For O—Al and O—Si pairs, in contrast, it increases with increasing of nanoparticle size and it is larger than that for the bulk (see Table 1). We also found the changes in tricluster distributions with a size of amorphous AS_2 nanoparticles. For the bulk it was found that about 43% oxygen atoms are three-fold coordinated by (Al, Si) atoms [27]. In contrast, in the amorphous AS_2 nanoparticles, percentage of the O atoms with three-fold coordinated by (Si, Al) atoms is equal to 25, 28 and 31% for the sizes of 2, 3 and 4 nm, respectively. Cation compositions of the triclusters are shown in Table 2. These triclusters have an important role for the explanation of structure and properties of aluminosilicate melts and glasses such as it might be responsible for the facilitation of diffusion or several viscosity trends in nanoparticles similarly to those discussed for the bulk [35].

On the other hand, more information about local structure of nanoparticles can be found via the most important bond-angle distributions such as O—Al—O, Al—O—Al, and analogously O—Si—O and Si—O—Si angles. From Figure 2, we can see that such distributions also depend on the size of nanoparticles due to the surface effects. For nanoparticles with the size of 3 and 4 nm, the main peak of distribution for O—Al—O angle is at 105.3° which is close to that for O—Si—O angle, i.e. it is equal to 106°, and close to those for the tetrahedral network structure. In contrast, for Al—O—Al angle it is at around 94.3° and it is much less than that of Si—O—Si angle which is equal to 165°. This indicates that the packing of AlO_n units in the AS_2 system is denser than those of SiO_n units. On the other hand, the main peaks in such bond-angle distributions are located at around the values close to those for ideal tetrahedra like those discussed above [31,32].

Another important structural quantity of nanoparticle is the dependence of particle density $\rho(R)$ on the distance R from the center of nanoparticle [36]. This quantity is determined as follows: we find the number of atoms belonging to the spherical shell with the thickness of 0.20 Å formed by two spheres with the radii of $R - 0.10$ Å and $R + 0.10$ Å. Then we calculate the quantity $\rho(R)$ for the finite large enough value, i.e. $R \geq 5.0$ Å, like that done in [37] and the local density is a rather noisy variable (Figure 3). As shown in Figure 3, $\rho(R)$ fluctuates around the value of 2.6 g cm^{-3} which is equal to the density of an amorphous AS_2 obtained in previous works [30]. Strong fluctuations of $\rho(R)$ indicate that our statistics are not good, smoother changes of the curves can be obtained via averaging over many independent runs. Furthermore, in order to gain more insights into the surface structure of nanoparticles we show the partial atomic density profiles

Table 2. Composition of triclusters.

	Number of Al atoms in triclusters			
Material	0 (%)	1 (%)	2 (%)	3 (%)
2 nm	0	9	60.2	30.8
3 nm	0.5	9.4	55.3	34.8
4 nm	0.4	10.2	56.5	32.9
Bulk [27]	1.1	16.2	56.8	25.9

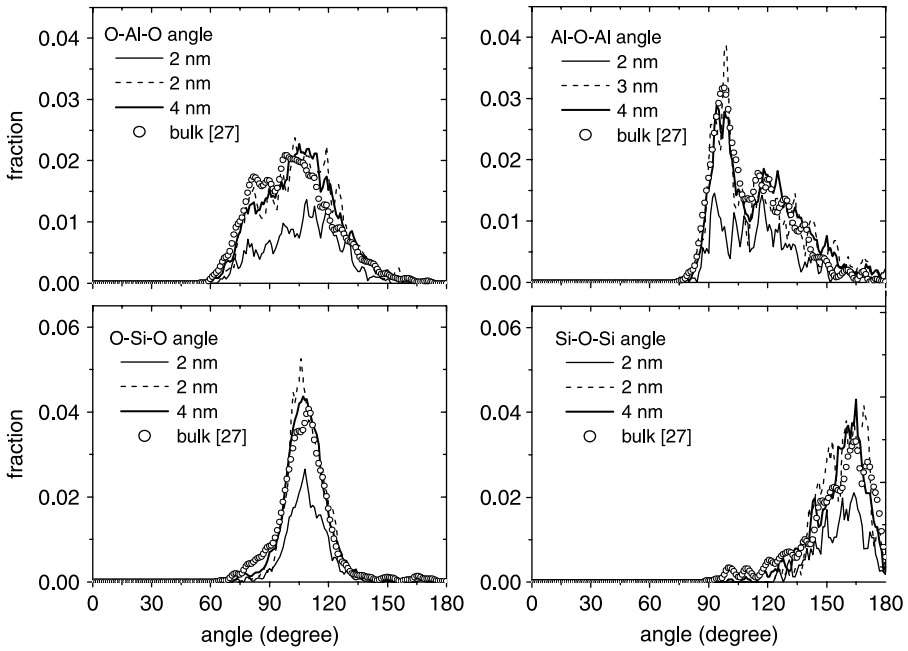

Figure 2. Bond-angle distributions in amorphous AS_2 nanoparticles.

for Al, Si and O atoms separately in Figure 4. One can see that O atoms have tendency to concentrate at the surface of nanoparticles like those observed at the liquid SiO_2 or amorphous Al_2O_3 surfaces [11,13]. The reason for such phenomenon is that the system is energetically better to have O atoms at the surface because only one bond has to be broken. However, Al atoms, $Z_{Al} = +3$, also have a tendency to concentrate at the surface together with O ones may be for a partial charge neutrality since Si atoms have no such tendency. One can see that the distributions of different atomic species at the surface of amorphous AS_2 nanoparticles are more complicated compared with those observed at the liquid SiO_2 or amorphous Al_2O_3 surfaces at which the cations have a tendency to concentrate at the layers just below the surface in order to achieve the local charge neutrality [11,13]. The phenomenon may be related to the contribution of topological effects on the rearrangement of atoms at the surface of AS_2 nanoparticles due to the presence of atoms of different sizes and charges in multicomponent system. It seems that the peak of the total density in the vicinity of the surface of AS_2 nanoparticles also occurs like that found in liquid SiO_2 or amorphous Al_2O_3 nanosized systems (see Figure 3 and [11,13,36]). However, unlike those observed in [11,13,36] the density profile curves in our amorphous AS_2 do not decrease down to zero at the surface (Figure 3). This may related to the different boundary conditions used in simulations. In the present work, we use the non-periodic boundary conditions with non-elastic reflection behavior, i.e. during the relaxation process if atoms move out from the boundary of spherical nanoparticles those atoms have to be located right at the surface. Hence, significant amount of atoms in our nanoparticles concentrates right at the surface.

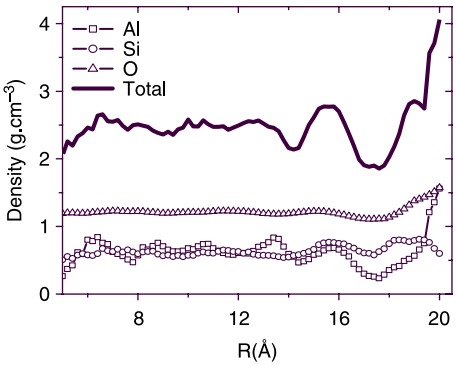

Figure 3. Density profile in amorphous AS_2 nanoparticles.

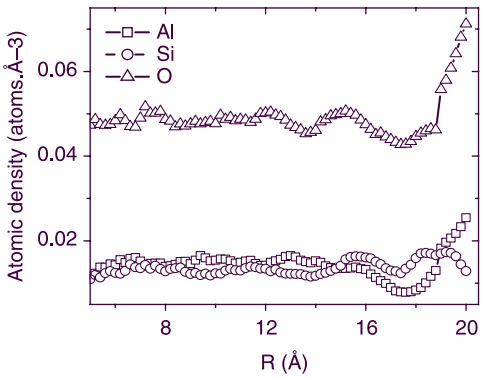

Figure 4. Atomic density profile in amorphous AS_2 nanoparticle at 350 K.

Table 3. The mean coordination number in the surface shell and in the core of nanoparticles at the temperature of 350 K.

Materials		Z_{Al-Al}	Z_{Al-Si}	Z_{Si-Al}	Z_{Si-Si}	Z_{Al-O}	Z_{O-Al}	Z_{Si-O}	Z_{O-Si}	Z_{O-O}
2 nm	Surface	2.53	2.25	2.45	2.12	3.48	1.40	4.05	1.36	6.85
	Core	3.70	3.00	3.13	2.33	4.35	1.79	4.06	1.34	8.83
3 nm	Surface	2.20	2.35	2.38	2.13	3.51	1.34	4.01	1.37	6.92
	Core	4.00	2.82	3.06	2.39	4.38	1.84	4.08	1.34	9.47
4 nm	Surface	2.87	2.31	2.54	2.13	3.68	1.46	4.01	1.37	7.15
	Core	3.81	2.95	3.04	2.44	4.00	1.78	4.09	1.37	9.39

Furthermore, we found that concentration of structural defects at the surface increases with decreasing nanoparticle size. In order to clarify structural changes and the concentration of surface defects in nanoparticles with different sizes, we show the mean coordination number for different atomic pairs in the core and in the 3.19 Å top spherical shells of nanoparticles in Table 3. Indeed, structural properties of surface and core strongly depend on the size of nanoparticles. First, in the surface shells, the mean coordination number for different atomic pairs increases with increasing of size with an exception for Z_{Si-O}. The surface mean coordination number for Si—O pairs decreases from 4.05 to 4.01 and these values are close to that for an ideal tetrahedron. In contrast, for Al—O pair it is much smaller than the value of 4.00, which indicates a large number of under-coordinated Al atoms to oxygen. This is relating to the domination of the point defects in the surface layer of amorphous AS_2 nanoparticles. These surface defects can play an important role in structure and properties of nanoparticles and determination of the relationship between atomic surface structure and other physicochemical properties of nanomaterials is one of the most important achievements of surface science [38–41]. In contrast, the mean coordination number for the Al—O and Si—O pairs in the core of nanoparticles is larger than that in the surface layer and is around the value of 4.00. Moreover, mean coordination number for other atomic pairs in the core of nanoparticles is also higher than those in the surface layer indicated the differences between structures of the core and surface of nanoparticles.

Finally, we would like to show the thermodynamic quantities of amorphous AS_2 nanoparticles. Our calculations show that E_{pot} for nanoparticles, i.e. the potential energy of the systems, is significantly higher than that for the bulk one due to the surface energy of the formers. Thus, we can suggest the relation: $E_{pot}^{nano} - E_{pot}^{bulk} = E_s$. Here, E_s is the surface energy of nanoparticles [11]. In the present work, we calculated the value for E_s only for the models obtained at 350 K after relaxation of 50,000 MD steps. E_s is equal to 0.456 J m^{-2}, 0.442 J m^{-2}, 0.429 J m^{-2} for the size of 2, 3 and 4 nm, respectively. It seems that E_s has a tendency to decrease with increasing nanoparticle size like those observed for amorphous TiO_2 nanoparticles [42]. Although there is no experimental and calculated data for the surface energy of amorphous AS_2 nanoparticles to compare, one can consider that the calculated E_s has a reasonable value, which is close to those obtained by calculations and experiments for SiO_2 nanoclusters or Al_2O_3 thin films, which is equal to 0.67 and 0.88 J m^{-2}, respectively [36,43].

4. Conclusions

Structural properties and thermodynamic quantities of amorphous AS_2 nanoparticles at three different sizes were studied via MD simulation with the Born-Mayer type pair potentials. The conclusions can be drawn as following:

Via calculations for structural quantities such as interatomic distances, PRDFs, coordination numbers and bond-angle distributions at 350 K for three different sizes, we found that the amorphous AS_2 nanoparticles have a slightly distorted tetrahedral network structure in which Si and Al are mainly surrounded by four oxygen atoms. However, these results are different from those observed in the bulk although tetrahedral network structure also remains in nanosized systems.

We found a strong size dependence of the surface structure of nanoparticles and it differs from that of the core, i.e. the mean coordination number for different atomic pairs in the former is smaller than that in the latter due to the surface effects. We found that O atoms have a tendency to concentrate at the surface and the same tendency was found for Al atoms while Si atoms have no such tendency. This indicates a complex atomic arrangement at the surface of amorphous AS_2 nanoparticles, which may be due to the topological effects caused by the presence of atoms of different sizes and charges in multicomponent system.

Moreover, size effects on the surface energy of amorphous AS_2 nanoparticles were found, i.e. surface energy decreases with increasing nanoparticle size. The calculated surface energy of AS_2 nanoparticles has a reasonable value, which is close to that obtained for SiO_2 and Al_2O_3 nanosized systems.

References

[1] E. Gavilan et al., *One-pot synthesis of Fluorescent Porous Aluminosilicate Nanoparticles*, Comp. Ren. Chimie 8 (2004), p. 1946.

[2] A. Sakamoto, F. Sato, and S. Yamamoto, *Structural relaxation and optical properties in transparent nanocrystalline β-quartz glass-ceramic*, J. Non-Cryst, Solid 352 (2006), p. 514.

[3] B. Došová et al., *Sorption of As^{V} on aluminosilicates treated with Fe^{II} nanoparticles*, J. Colloid and Interf. Sci. 302 (2006), p. 424.

[4] Y. Liu and T.J. Pinnavaia, *Aluminosilicate Nanoparticles for Catalytic Hydrocarbon Cracking*, J. Am. Chem. Soc. 125 (2003), p. 2376.

[5] K.S. Triantafyllidis et al., *Gas-oil cracking activity of hydrothermally stable aluminosilicate mesostructures (MSU-S) assembled from zeolite seeds: Effect of the type of framework structure and porosity*, Catal. Today 112 (2006), p. 33.

[6] J. Leivo et al., *Sol-gel synthesis of a nanoparticulate aluminosilicate precursor for homogeneous mullite ceramics*, J. Mater. Res. 21 (2006), p. 1279.

[7] C. Zha and G.R. Atkins, *Preparation and Spectroscopy of Aluminosilicate Films Deposited on Graphite Surfaces via an Anhydrous Sol-Gel Route*, J. Sol–Gel Sci. Tech. 19 (2000), p. 741.

[8] Y.F. Tang et al., *Study on the densification of composite coating particles of a-Al_2O_3-SiO_2*, Mater. Chem. Phys. 75 (2002), p. 265.

[9] G.J. Kramer, A.J.M. de Man, and R.A. van Saten, *Zeolites versus aluminosilicate clusters: the validity of a local description*, J. Am. Chem. Soc. 113 (1991), p. 6435.

[10] P.M. Oliver et al., *Atomistic simulation of the surface structure of the TiO_2 polymorphs rutileand anatase*, J. Mater. Chem. 7 (1997), p. 563.

[11] A. Roder, W. Kob, and K. Binder, *Structure and dynamics of amorphous silica surfaces*, J. Chem. Phys. 114 (2001), p. 7602.

[12] R.C. Baetzold and H. Yang, *Computational Study on Surface Structure and Crystal Morphology of γ-Fe_2O_3: Toward Deterministic Synthesis of Nanocrystals*, J. Phys. Chem. B 107 (2003), p. 14357.

[13] S.P. Adiga, P. Zapol, and L.A. Curtiss, *Atomistic simulations of amorphous alumina surfaces*, Phys. Rev. B 74 (2003), p. 064204.

[14] J.F. MacDowell and G.H. Beall, *Immiscibility and Crystallization in Al_2O_3-SiO_2 Glasses*, J. Am. Ceram. Soc. 52 (1969), p. 17.

[15] I.A. Aksay, J.A. Pask, and R.F. Davis, *Densities of SiO_2-Al_2O_3 Melts*, J. Am. Ceram. Soc. 62 (1979), p. 332.

[16] S.H. Risbud et al., *Solid-state NMR Evidence of 4-, 5, and 6-Fold Aluminum Sites in Roller-Quenched SiO_2-Al_2O_3 Glasses*, J. Am. Ceram. Soc. 70 (1987), p. C10.

[17] P. McMillan and B. Piriou, *The structures and vibrational spectra of crystals and glasses in the silica-alumina system*, J. Non-Cryst. Solids 53 (1982), p. 279.

[18] B.T. Poe et al., *Silica-alumina liquids: in-situ study by high-temperature aluminum-27 NMR spectroscopy and molecular dynamics simulation*, J. Phys. Chem. 96 (1992), p. 8220.

[19] S. Sen and J.F. Stebbins, *Structural role of Nd^{3+} and Al^{3+} cations in SiO_2 glass: α^{29}Si MAS-NMR spin-lattice relaxation, ^{27}Al NMR and EPR study*, J. Non-Cryst. Solids 188 (1995), p. 54.

[20] M. Schmucker et al., *NMR studies on rapidly solidified SiO_2-Al_2O_3 and SiO_2-Al_2O_3-Na_2O-glasses*, J. Non-Cryst. Solids 217 (1997), p. 99.

[21] J.F. Stebbins and Z. Xu, *NMR evidence for excess non-bridging oxygen in an aluminosilicate glass*, Nature London 390 (1997), p. 60.

[22] M. Schmucker et al., *Comparative ^{27}Al NMR and LAXS studies on rapidly quenched aluminosilicate glasses*, J. Eur. Ceram. Soc. 19 (1999), p. 99.

[23] S.K. Lee and J.F. Stebbins, *The Structure of Aluminosilicate Glasses: High-Resolution ^{17}O and ^{27}Al MAS and 3QMAS NMR Study*, J. Phys. Chem. B 104 (2000), p. 4091.

[24] M. Schmucker and H. Schneider, *New evidence for tetrahedral triclusters in aluminosilicate glasses*, J. Non-Cryst. Solids 311 (2002), p. 211.

[25] S. Sen and R.E. Youngman, *High-Resolution Multinuclear NMR Structural Study of Binary Aluminosilicate and Other Related Glasses*, J. Phys. Chem. B 108 (2004), p. 7557.

[26] M. Okuno et al., *Structure of SiO_2-Al_2O_3 glasses: Combined X-ray diffraction, IR and Raman studies*, J. Non-Cryst. Solids 351 (2005), p. 1032.

[27] V.V. Hoang, N.N. Linh, and N.H. Hung, *Structure and dynamics of liquid and amorphous Al_2O_3.2SiO_2*, Eur. Phys. J. Appl. Phys. 37 (2007), p. 111.

[28] V.W. Hoang, *Composition dependence of static and dynamic heterogeneities in simulated liquid aluminum silicates*, Phys. Rev. B 75 (2007), p. 174202.

[29] N.N. Linh and V.V. Hoang, *Structural properties of simulated liquid and amorphous aluminium silicates*, Phys. Scr. 76 (2007), p. 165.

[30] A. Winkler et al., *Structure and diffusion in amorphous aluminum silicate: A molecular dynamics computer simulation*, J. Chem. Phys. 120 (2004), p. 384.

[31] V.V. Hoang, D.K. Belashchenko, and V.T.M. Thuan, *Computer simulation of the structural and thermodynamics properties of liquid and amorphous SiO_2*, Physica B 348 (2004), p. 249.

[32] V.V. Hoang, *Molecular dynamics study on structure and properties of liquid and amorphous Al_2O_3*, Phys. Rev. B 70 (2004), p. 134204.

[33] D. Nevins and F.J. Spera, *Molecular dynamics simulations of molten $CaAl_2Si_2O_8$: Dependence of structure and properties on pressure*, Am. Mineral. 83 (1998), p. 1220.

[34] M. Benoit, S. Ispas, and M.E. Tuckerman, *Structural properties of molten silicates from ab initio molecular-dynamics simulations: Comparison between CaO-Al_2O_3-SiO_2 and SiO_2*, Phys. Rev. B 64 (2001), p. 224205.

[35] V.V. Hoang, *Local environments of oxygen in $Al_2O_3SiO_2$ melts*, Phys. Lett. A 368 (2007), p. 499.

[36] I.V. Schweigert et al., *Structure and properties of silica nanoclusters at high temperatures*, Phys. Rev. B 65 (2002), p. 235410.

[37] J. Huang and L.S. Bartell, *Structure and properties of potassium iodide nanoparticles. A molecular dynamics study*, Mol. Structure 567 (2000), p. 145.

[38] Y. Kuroda, T. Mori, and Y. Yoshikawa, *Improvement in the surface acidity of Al_2O_3·SiO_2 due to a high Al dispersion*, Chem. Commun. 11 (2001), p. 1006.

[39] P.J. O'Malley and J. Dwyer, *An ab initio quantum chemical investigation on the effect of the magnitude of the T-O-T angle on the Broensted acid characteristics of zeolites*, J. Phys. Chem. 92 (1988), p. 3005.

[40] G. Sastre, V. Fornes, and A. Corma, *Preferential Siting of Bridging Hydroxyls and their Different Acid Strengths in the Two-Channel System of MCM-22 Zeolit*, J. Phys. Chem. B 104 (2000), p. 4349.

[41] V.L. Parola et al., *Effect of the Al/Si atomic ratio on surface and structural properties of sol-gel prepared aluminosilicates*, J. Solid State Chem. 174 (2003), p. 482.

[42] V.V. Hoang, H. Zung, and N.H.B. Trong, *Structural properties of simulated liquid and amorphous aluminium silicates*, Eur. Phys. J. D 44 (2007), p. 515.

[43] J. Mizele, J.L. Dandurand, and J. Schott, *Determination of the surface energy of amorphous silica from solubility measurements in micropores*, Surf. Sci. 162 (1985), p. 830.